Available online at www.sciencedirect.com

SciVerse ScienceDirect

Ceramics International 39 (2013) 7537–7544

CERAMICS INTERNATIONAL

www.elsevier.com/locate/ceramint

Formation of MAX solid solutions $(Ti,V)_2AlC$ and $(Cr,V)_2AlC$ with Al_2O_3 addition by SHS involving aluminothermic reduction

C.L. Yeh*, W.J. Yang

Department of Aerospace and Systems Engineering, Feng Chia University, 100 Wenhwa Road, Seatwen, Taichung 40724, Taiwan

Received 31 December 2012; received in revised form 6 February 2013; accepted 2 March 2013
Available online 14 March 2013

Abstract

MAX solid solutions $(Ti,V)_2AlC$ and $(Cr,V)_2AlC$ with Al_2O_3 addition were produced by solid state combustion involving aluminothermic reduction in the mode of self-propagating high-temperature synthesis (SHS). Starting materials included $TiO_2/V_2O_5/Al/Al_4C_3$ and $Cr_2O_3/V_2O_5/Al/Al_4C_3$ powder mixtures. Attempts were made to attain $(Ti_{1-x}V_x)_2AlC$ and $(Cr_{1-y}V_y)_2AlC$ with the V content in terms of x and y from 0.1 to 0.7. Combustion exothermicity was increased by increasing V_2O_5 for the yield of a higher proportion of V at the substitution site, which not only increased the combustion temperature and reaction front velocity, but also facilitated the evolution of solid solutions. Due to insufficient reaction exothermicity, $(Ti_{1-x}V_x)_2AlC/Al_2O_3$ in situ composites were only produced under $x \geq 0.4$. On the other hand, the formation of $(Cr_{1-y}V_y)_2AlC/Al_2O_3$ was achieved with y from 0.1 to 0.7, because reduction of Cr_2O_3 is more energetic than that of TiO_2. The laminated microstructure characteristic of the MAX ternary carbide was observed for both Al_2O_3-added $(Ti,V)_2AlC$ and $(Cr,V)_2AlC$ composites synthesized in this study.

Keywords: A. Powders: solid state reaction; B. Platelets; C. Toughness and toughening; Ternary carbide solid solutions; Self-propagating high-temperature synthesis (SHS)

1. Introduction

The $M_{n+1}AX_n$ phases, where M is an early transition metal, A is an A-group (mostly IIIA and IVA) element, X is either C or N, and $n=1$, 2, or 3, are a new class of materials featuring a crystal structure of hexagonal symmetry [1–4]. Both MAX ternary carbides and nitrides possess unique properties combining many merits of metals and ceramics, including low density, high modulus, good thermal and electrical conductivities, excellent thermal shock and oxidation resistance, damage tolerance, and easy machinability [5–9]. These characteristics stem from an inherently laminated crystal structure with the $M_{n+1}X_n$ slabs intercalated with pure A-element layers [4]. Moreover, the solid solutions based on MAX phases can be formed by partial substitution of elements at the M, A, or X site, and such a treatment provides a strengthening effect and renders great potential for tailoring and/or optimizing the properties of the resulting products [10–12].

Schuster et al. [13] firstly studied the solid solution of $(M_{1-x}M'_x)_2AlC$, in which M and M′ can be Ti, Cr, or V, by annealing Ti_2AlC, Cr_2AlC, and V_2AlC powders of different quantities at 1000 °C for 170 h in an evaluated quartz tube. Except for the Ti_2AlC/Cr_2AlC system, both $(Ti,V)_2AlC$ and $(Cr,V)_2AlC$ solid solutions with V proportions at 0.25, 0.5, and 0.75 were obtained [13]. A theoretical investigation by Sun et al. [14] on the solubility of $(M_{1-x}M'_x)_2AlC$ confirmed the experimental observations of Schuster et al. [13]. Other fabrication routes, like hot isostatic pressing (HIP), hot pressing (HP), and pulse discharge sintering (PDS), have been adopted for the preparation of various MAX solid solutions.

Gupta and Barsoum [15] fabricated $(Ti_{0.5}V_{0.5})_2AlC$ by HIP at 1600 °C and 100 MPa for 8 h from the powder mixture composed of Ti, V, Al, and graphite. In the same way, Salama et al. [16] obtained $(Ti,Nb)_2AlC$ with a Ti:Nb ratio close to 1:1 using the mixture of Ti, Nb, Al_4C_3, and graphite powders. By in situ hot pressing/solid–liquid reaction, Meng et al. [17] prepared

*Corresponding author. Tel.: +886 4 24517250x3963; fax: +886 4 24510862.
E-mail address: clyeh@fcu.edu.tw (C.L. Yeh).

0272-8842/$ - see front matter © 2013 Elsevier Ltd and Techna Group S.r.l. All rights reserved.
http://dx.doi.org/10.1016/j.ceramint.2013.03.005

$(Ti,V)_2AlC$ with 5–20 at% of V in the substitution site from the elemental powders at 1450 °C and 100 MPa for 60 min. The strengthening effect resulting from the replacement of a fraction of Ti with V on Ti_2AlC was also examined [17]. The PDS technique was utilized by Tian et al. [18] to synthesize $(Cr_{1-x}V_x)_2AlC$ (with $x=0.1$, 0.25, and 0.5) from elemental powders under 1250–1300 °C for 90 min. In addition, the production of many A- and X-site solid solutions, such as $Cr_2(Al,Si)C$, $Ti_3(Al,Si)C_2$, $Ti_3(Al,Sn)C_2$, and $Ti_3Al(C,N)_2$, has been conducted by HP and HIP [19–21].

The improvement of mechanical properties of the MAX carbides and their related solid solutions was also achieved by incorporating the second ceramic phase like Al_2O_3, TiB_2, and TiC [22–25]. For example, Zhu et al. [22] synthesized $(Ti,Nb)_2AlC/Al_2O_3$ in situ composites from Nb_2O_5, Ti, Al, and carbon black powders by HP at 1350 °C and 16 MPa for 2 h. With the addition of Al_2O_3, the increase of Vickers hardness, compressive stress, flexural strength, and fracture toughness was demonstrated [22]. Yang et al. [23] obtained the $Ti_3SiC_2/TiB_2/TiC$ composites with enhanced bending strength, fracture toughness, and Vickers hardness. Likewise, the reinforcing and toughening effects were observed for Ti_3AlC_2/Al_2O_3 and Ti_3AlC_2/TiB_2 composites [24,25].

As a promising alternative, combustion synthesis in the self-propagating high-temperature synthesis (SHS) mode takes advantage of the self-sustaining merit from highly exothermic reactions, and hence, has the benefits of low energy requirement, short processing time, and simple facilities [26,27]. Besides refractory materials (such as carbides, borides, and nitrides) and intermetallics (such as aluminides, titanides, and silicides), combustion synthesis of the SHS mode has been applied to fabricate a variety of MAX compounds, including Ti_2AlC, Ti_3AlC_2, Ti_2AlN, and Cr_2AlC [28–30]. Recently, successful attempts were made on the production of the MAX solid solutions, $Ti_3(Al,Si)C_2$ [31] and $Ti_2Al(C,N)$ [32].

Of particular interest for this work are two M-site MAX solid solutions, $(Ti,V)_2AlC$ and $(Cr,V)_2AlC$, because both of them have not been investigated by combustion synthesis. Moreover, this study aims to combine aluminothermic reduction of TiO_2, V_2O_5, and Cr_2O_3 (i.e., thermite reactions) into the SHS process for in situ formation of Al_2O_3-added $(Ti,V)_2AlC$ and $(Cr,V)_2AlC$. The highly exothermic nature of the thermite reaction is a great benefit to solid state combustion, and the use of metal oxides as the source of metallic elements gain the cost-effective merit. As the first attempt, both $(Ti_{1-x}V_x)_2AlC$ and $(Cr_{1-y}V_y)_2AlC$ with a broad atomic proportion at the substitution site were produced by self-sustaining combustion. The effects of the sample stoichiometry were studied on the phase composition of the synthesized product, as well as on the sustainability of the combustion wave, flame-front velocity, and combustion temperature.

2. Experimental methods of approach

The starting materials adopted by this study included TiO_2 (Showa Chemical, 99%), V_2O_5 (Showa Chemical, 99%), Cr_2O_3 (Showa Chemical, 99%), Al (Showa Chemical, <40 μm, 99%), and Al_4C_3 (Strem Chemicals, <45 μm, 98%) powders. The reactant mixtures were formulated with stoichiometries according to Reactions (1) and (2) respectively for the preparation of $(Ti,V)_2AlC/Al_2O_3$ and $(Cr,V)_2AlC/Al_2O_3$ in situ composites.

$$2(1-x)TiO_2 + xV_2O_5 + \left(\frac{2x+7}{3}\right)Al + \frac{1}{3}Al_4C_3 \rightarrow (Ti_{1-x}V_x)_2AlC + \left(\frac{x+4}{3}\right)Al_2O_3 \quad (1)$$

$$(1-y)Cr_2O_3 + yV_2O_5 + \left(\frac{4y+5}{3}\right)Al + \frac{1}{3}Al_4C_3 \rightarrow (Cr_{1-y}V_y)_2AlC + \left(\frac{2y+3}{3}\right)Al_2O_3 \quad (2)$$

where the stoichiometric parameters x and y represent the V content at the substitution site of $(Ti_{1-x}V_x)_2AlC$ and $(Cr_{1-y}V_y)_2AlC$, and the values of x and y in the range from 0.1 to 0.7 are considered in this study. It should be noted that Reactions (1) and (2) involve aluminothermic reduction of metal oxides, including TiO_2, Cr_2O_3, and V_2O_5. Thermite reactions based upon Al as the reducing agent are recognized by the release of a large amount of heat and formation of a stable oxide Al_2O_3. The reaction enthalpy per one mole of Al_2O_3 formed generated from aluminothermic reduction of TiO_2, Cr_2O_3, and V_2O_5 is 258.7, 541.0, and 745.6 kJ, respectively [33]. This means that the most energetic reduction of V_2O_5 should lead to an increase in combustion exothermicity of Reactions (1) and (2) for the formation of solid solutions with a higher vanadium proportion.

After sufficiently blending in a ball mill, the reactant powders were cold-pressed into the cylindrical compact with a diameter of 7 mm, a height of 12 mm, and a compaction density of 55% relative to the theoretical maximum density (TMD). The SHS experiment was performed in a stainless-steel windowed chamber under an atmosphere of high purity argon (99.99%). Details of the experimental setup and measurement approach to the combustion variables were reported elsewhere [34]. In this study, the fracture toughness (K_{IC}) was determined by the indentation method using the following equation proposed by Evans and Charles [35].

$$K_{IC} = 0.16 H_v a^{1/2} \left(\frac{c}{a}\right)^{-3/2} \quad (3)$$

where H_v is the Vickers hardness, a the half of the average length of two diagonals of the indentation, and c the radial crack length measured from the center of the indentation. A schematic description of these parameters associated with the Vickers indentation can be found in Ref. [36]. The Vickers hardness (H_v) was evaluated from the applied load ($P=9.8$ N) and the diagonal length d ($=2a$) of the indentation, as expressed by the equation below.

$$H_v = 1.8544 \frac{P}{d^2} \quad (4)$$

3. Results and discussion

3.1. Observation of combustion characteristics

Two typical combustion sequences illustrated in Fig. 1(a) and (b) were recorded from the reactant compacts of Reaction (1) with $x=0.3$ and 0.7, respectively. For the sample shown in Fig. 1(a), a distinct combustion wave forms upon ignition and propagates as a localized hot spot along a spiral trajectory in a self-sustaining manner. It is obvious that the sample almost retains its original shape except for some crevices generated by the spinning motion of the reaction zone. On the other hand, Fig. 1(b) reveals a nearly planar combustion front spreading rapidly from the ignited top plane to the bottom of the compact. Besides, propagation of the combustion wave is accompanied with massive melting of the burned sample. It is believed that the difference in combustion exothermicity between two samples is responsible for the dissimilar combustion behavior observed above. According to Ivleva and Merzhanov [37], the appearance of the spinning combustion wave is caused by the fact that the heat flux liberated from self-sustaining combustion is no longer sufficient to maintain steady propagation of a planar reaction front; therefore, combustion is confined to one or several localized reaction zones. Considerable melting of the burned sample is attributed to the increase of combustion exothermicity with an increment in the V_2O_5 content of the powder mixture, which increases the combustion temperature exceeding the melting points of some reactants and products. The increase of the parameter x signifies the powder mixture containing not only a larger amount of V_2O_5 but more Al. Low melting points of both V_2O_5 (679 °C) and Al (660 °C) could be another cause aggravating the melting of the sample observed in Fig. 1(b).

According to experimental observations, no combustion was initiated for the samples of Reaction (1) with $x=0.1$ and 0.2 because mainly of inadequate reaction exothermicity. With the increase of V_2O_5 and Al, the SHS process featuring a spinning reaction zone was observed for the powder compacts with $x=0.3$ and 0.4, beyond which the planar combustion front developed and melting of the sample occurred. Since aluminothermic reduction of Cr_2O_3 was more energetic than that of TiO_2, self-sustaining combustion in a spinning mode was found on the formation of $(Cr_{1-y}V_y)_2AlC/Al_2O_3$ composites from Reaction (2) with $y=0.1$ and 0.2. For the samples formulated with y from 0.3 to 0.7, the increase of reaction exothermicity facilitated the steady propagation of the planar combustion wave. Likewise, the reactant compact intended for the Al_2O_3-added $(Cr_{1-y}V_y)_2AlC$ solid solution with a higher atomic ratio of V to Cr experienced more substantial melting during the SHS process.

3.2. Measurement of flame-front propagation velocity and combustion temperature

Fig. 2 presents the variations of flame-front propagation velocity (V_f) with the V content of Al_2O_3-added $(Ti_{1-x}V_x)_2AlC$

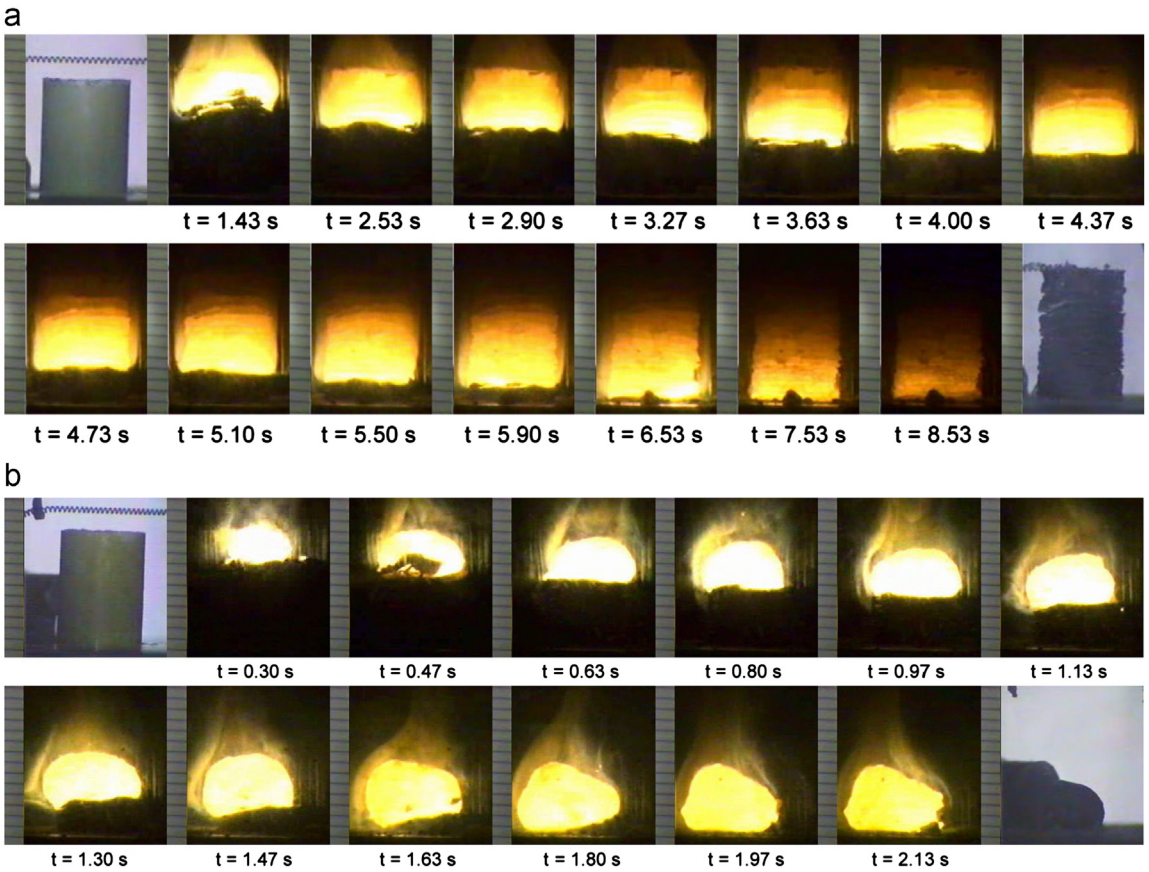

Fig. 1. Recorded images illustrating self-propagating combustion along sample compacts for formation of Al_2O_3-added $(Ti_{1-x}V_x)_2AlC$ with $x=$(a) 0.3 and (b) 0.7.

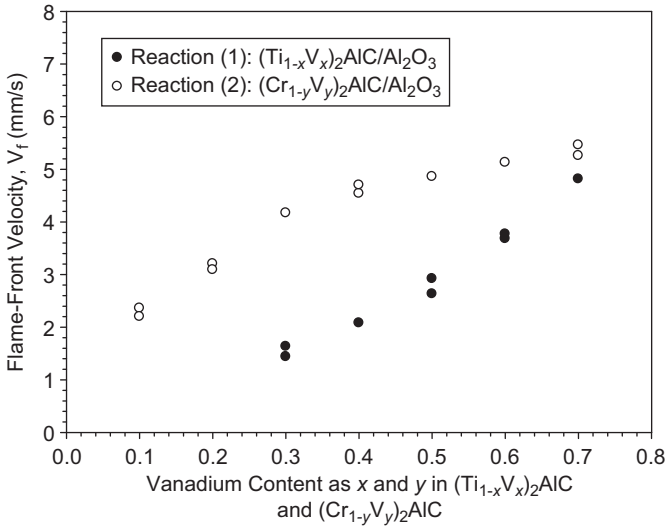

Fig. 2. Variations of flame-front propagation velocity with V content of Al_2O_3-added $(Ti_{1-x}V_x)_2AlC$ and $(Cr_{1-y}V_y)_2AlC$ synthesized by self-sustaining combustion.

and $(Cr_{1-y}V_y)_2AlC$ synthesized from Reactions (1) and (2), respectively. The reaction front velocity of Reaction (1), as shown in Fig. 2, increases from 1.4 to 4.8 mm/s for the formation of $(Ti_{1-x}V_x)_2AlC$ with the V content from $x=0.3$ to 0.7. On the preparation of the $(Cr_{1-y}V_y)_2AlC/Al_2O_3$ composites with $y=0.1$–0.7, the combustion wave velocity in the range of 2.2–5.5 mm/s was detected and the increase of the flame-front velocity with increasing V ratio was apparent. For both types of the samples, the increase of the combustion velocity is attributed to the larger amounts of V_2O_5 and Al adopted in the reactant mixture.

As also shown in Fig. 2, the flame-front velocity of Reaction (2) is higher than that of Reaction (1), but the gap between them narrows down for the formation of solid solutions with increasing vanadium content. The higher combustion velocity associated with formation of $(Cr_{1-y}V_y)_2AlC$ than $(Ti_{1-x}V_x)_2AlC$ is a consequence of a larger reaction enthalpy released from aluminothermic reduction of Cr_2O_3 than TiO_2. However, the influence of Cr_2O_3 gradually diminished as the amount of V_2O_5 increased for the formation of $(Ti,V)_2AlC$ and $(Cr,V)_2AlC$ with a higher V content at the substitution site.

Fig. 3(a) and (b) plots typical combustion temperature profiles of Reactions (1) and (2), respectively. As depicted in Fig. 3(a) and (b), the abrupt rise in temperature signifies the rapid arrival of the combustion wave and the peak value corresponds to the combustion front temperature. After the passage of the combustion front, an appreciable decrease in temperature is a result of dissipating heat to the surroundings. Fig. 3(a) indicates that the combustion front temperature increases from 1165 to 1550 °C as the parameter x of Reaction (1) increases from 0.3 to 0.7, confirming the increase of the reaction exothermicity with increasing V_2O_5 and Al. Similarly, as revealed in Fig. 3(b), the peak combustion temperature of Reaction (2) increases from 1212 to 1605 °C with increasing y value from 0.1 to 0.7. It is important to note that the dependence of the combustion temperature on sample stoichiometry is in a manner consistent with that of the reaction front velocity.

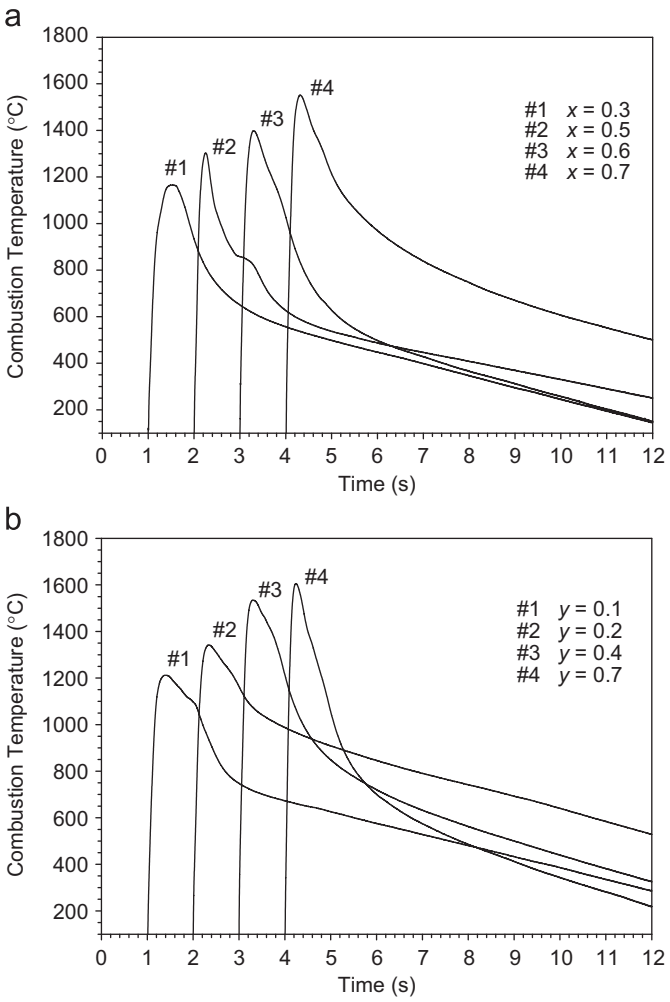

Fig. 3. Effects of V content of solid solutions on combustion temperature in association with SHS formation of Al_2O_3-added (a) $(Ti_{1-x}V_x)_2AlC$ and (b) $(Cr_{1-y}V_y)_2AlC$.

3.3. Composition and morphology analysis of combustion products

The XRD pattern of the product synthesized from Reaction (1) with $x=0.3$ is plotted in Fig. 4(a), which identifies the formation of a solid solution of binary carbides in the form of (Ti,V)C and an oxide Al_2O_3. Besides, there was a noticeable amount of elemental Al left unreacted in the final product. No formation of $(Ti,V)_2AlC$ was due most likely to the lack of sufficient reaction exothermicity, which thwarted further interactions between binary carbides and Al to yield MAX ternary carbides. For the powder compacts of Reaction (1) with $x=0.4$ and 0.7, the phase constituents of their respective products are unfolded in Fig. 4(b) verifying in situ formation of $(Ti,V)_2AlC$ and Al_2O_3. Moreover, as indicated by Fig. 4(b), the diffraction peaks of $(Ti,V)_2AlC$ shift to larger angles with the increment of the V content. For example, the position (2θ) of the (103) diffraction peak increases from 40.28° for $(Ti_{0.6}V_{0.4})_2AlC$ to 40.90° for $(Ti_{0.3}V_{0.7})_2AlC$. It is useful to note that the (103) peak position of Ti_2AlC is indexed at $2\theta=39.545°$ (JCPDS 29–0095) and that of V_2AlC at $2\theta=41.265°$ (JCPDS

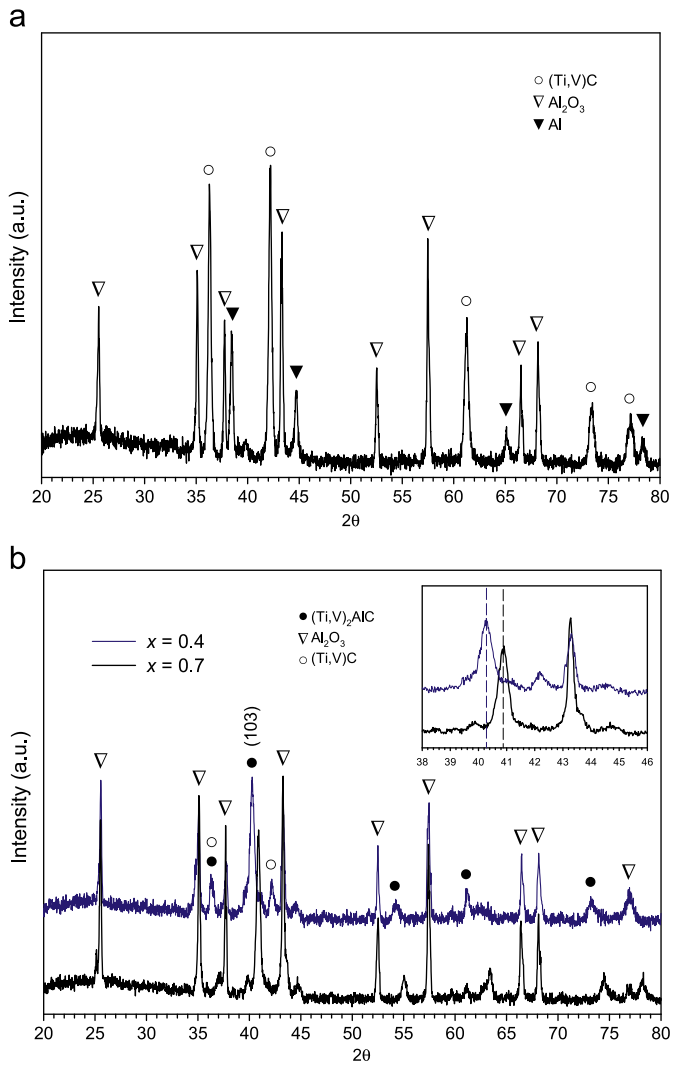

Fig. 4. XRD patterns of synthesized products for formation of Al_2O_3-added $(Ti_{1-x}V_x)_2AlC$ solid solution composites with (a) $x=0.3$ and (b) $x=0.4$ and 0.7.

29-0101), which interprets the variation of the diffraction angle of $(Ti,V)_2AlC$ with increasing ratio of V to Ti in the substitution site. According to Meng et al. [17], this is ascribed to the decrease of the lattice parameters. In addition, the intermediate phase (Ti,V)C was present in the case of $x=0.4$, but absent for $x=0.7$. This implies an improvement in the evolution of $(Ti_{1-x}V_x)_2AlC$ with increasing x value, due to the increase of the combustion exothermicity. The content of (Ti,V)C was estimated from the integrated XRD peak intensities according to Ref. [38]. The mass fraction of (Ti,V)C in the solid solution composites of $x=0.4$ and 0.5 was found to be 5.8–7.5 wt%.

From the XRD diffraction patterns, the lattice parameters, a and c, of $(Ti_{1-x}V_x)_2AlC$ solid solutions are calculated and listed in Table 1. Lattice constants of two end members, Ti_2AlC and V_2AlC, are also included for the comparison purpose. As summarized in Table 1, the lattice parameters decrease with increasing V content, because of the smaller size of the V atom in comparison to the Ti atom. The lattice

Table 1
Lattice parameters (a and c) for synthesized $(Ti_{1-x}V_x)_2AlC$ solid solutions.

Sample	a (Å)	c (Å)
Ti_2AlC [10]	3.065	13.710
$(Ti_{0.6}V_{0.4})_2AlC$	2.998	13.476
$(Ti_{0.5}V_{0.5})_2AlC$	2.981	13.432
$(Ti_{0.4}V_{0.6})_2AlC$	2.958	13.389
$(Ti_{0.3}V_{0.7})_2AlC$	2.946	13.348
V_2AlC [10]	2.914	13.190

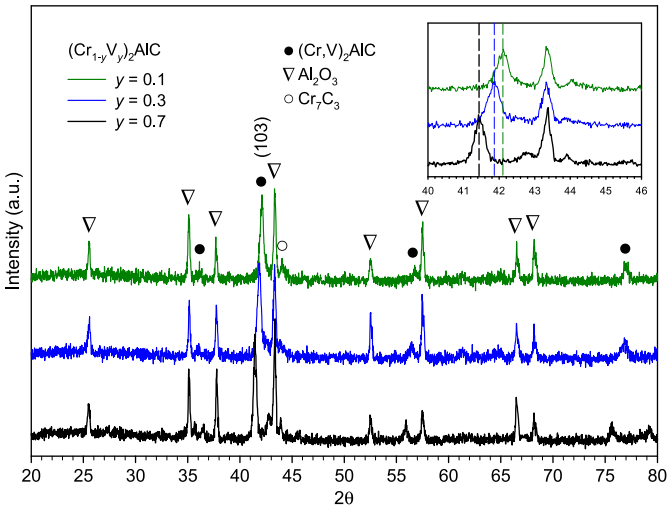

Fig. 5. XRD patterns of synthesized products for formation of Al_2O_3-added $(Cr_{1-y}V_y)_2AlC$ solid solution composites with $y=0.1$, 0.3, and 0.7.

Table 2
Lattice parameters (a and c) for synthesized $(Cr_{1-x}V_x)_2AlC$ solid solutions.

Sample	a (Å)	c (Å)
Cr_2AlC [18]	2.863	12.822
$(Cr_{0.9}V_{0.1})_2AlC$	2.867	12.842
$(Cr_{0.7}V_{0.3})_2AlC$	2.879	12.857
$(Cr_{0.5}V_{0.5})_2AlC$	2.889	12.934
$(Cr_{0.3}V_{0.7})_2AlC$	2.896	13.008
V_2AlC [10]	2.914	13.190

constants and their dependence on the V content at the substitution site agree well with the data in the literatures [10,17].

The XRD patterns of the products obtained from Reaction (2) with $y=0.1$, 0.3, and 0.7 are shown in Fig. 5. The formation of Al_2O_3-added $(Cr,V)_2AlC$ solid solution composites was confirmed. In proof of the different proportions of V formed in $(Cr,V)_2AlC$, Fig. 5 indicates that the diffraction peaks of $(Cr_{1-y}V_y)_2AlC$ shift to lower angles as the V content increases; for instance, the 2θ position of the (103) diffraction peak is indexed at 42.12° for $(Cr_{0.9}V_{0.1})_2AlC$, 41.88° for $(Cr_{0.7}V_{0.3})_2AlC$, and 41.42° for $(Cr_{0.3}V_{0.7})_2AlC$. The corresponding peaks of their end members are located at $2\theta=42.132°$ for Cr_2AlC (JCPDS 29-0017) and 41.265° for V_2AlC (JCPDS 29-0101), which justifies the shift to the lower

angle as the dissolution of V into the crystal lattice of Cr_2AlC increases. This is indicative of the increase of the lattice parameters [18]. In addition, a small amount of Cr_7C_3 was detected in the final product of $y=0.1$. Cr_7C_3 is considered as an intermediate for the formation of Cr_2AlC [30]. The content of Cr_7C_3 about 4.5–6.4 wt% was determined

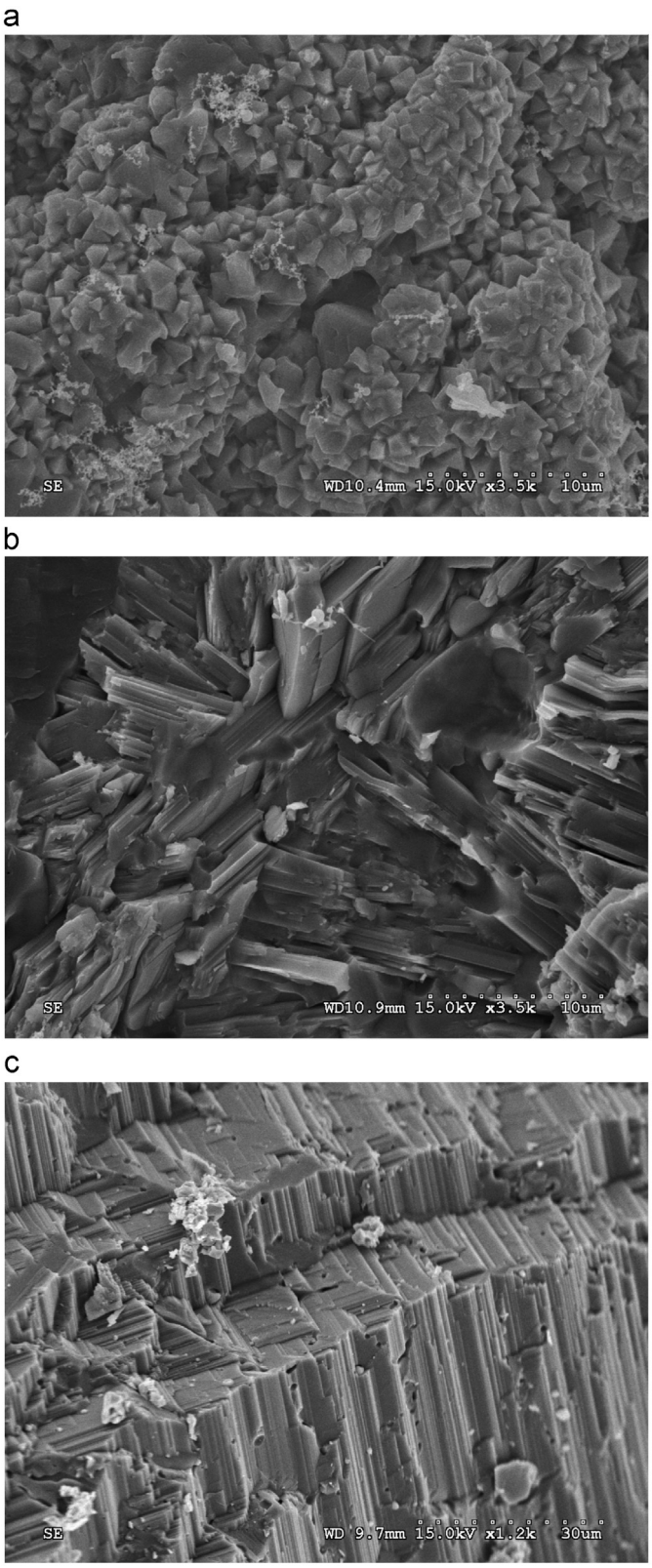

Fig. 6. SEM micrographs illustrating fracture surfaces of synthesized products of Al_2O_3-added $(Ti_{1-x}V_x)_2AlC$ with $x=$(a) 0.3, (b) 0.6, and (c) 0.7.

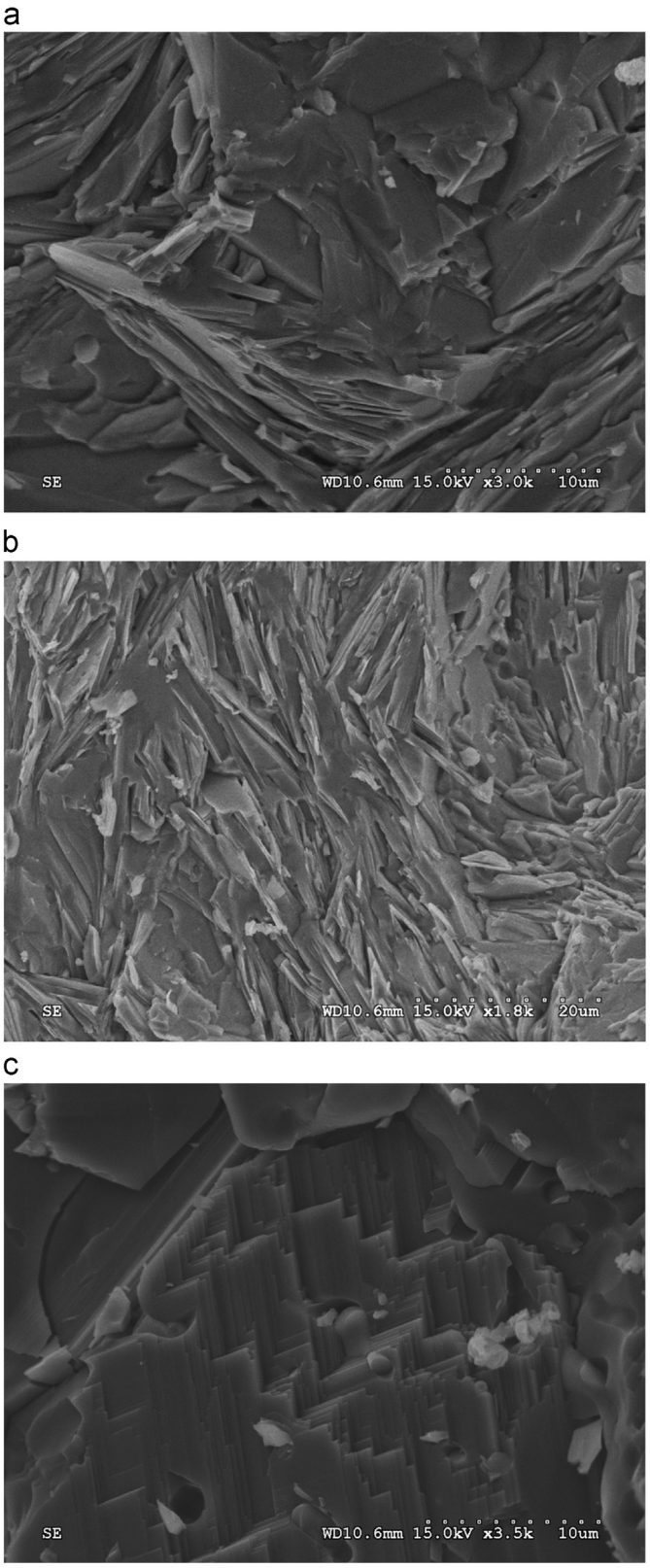

Fig. 7. SEM micrographs illustrating fracture surfaces of synthesized products of Al_2O_3-added $(Cr_{1-y}V_y)_2AlC$ with $y=$(a) 0.3, (b) 0.6, and (c) 0.7.

in the $(Cr_{1-y}V_y)_2AlC/Al_2O_3$ composites of $y=0.1$ and 0.2. No presence of Cr_7C_3 in the end products of Reaction (2) with $y\geq0.3$ suggests a better degree of the phase transformation.

Table 2 lists the lattice parameters of $(Cr_{1-y}V_y)_2AlC$ solid solutions with different V proportions and two corresponding end members. In contrast to $(Ti,V)_2AlC$, the lattice parameters of $(Cr,V)_2AlC$ increase with increasing V content. The larger atom size of V than Cr is responsible for the increase of the lattice parameters. According to Tian et al. [18], the more significant increment in c is attributed to the weaker electronic bonding in the c direction.

Fig. 6(a) and (b) illustrates the microstructure of fracture surfaces of the products synthesized from Reaction (1) with $x=0.3$ and 0.6, respectively. Agglomeration of small equiaxed (Ti,V)C grains of about 1–2 μm is evident in Fig. 6(a). Different from that observed in Fig. 6(a), laminar $(Ti,V)_2AlC$ grains with a thickness of 0.3–0.8 μm are clearly seen in Fig. 6 (b). The plate-like $(Ti,V)_2AlC$ grains are closely stacked into a laminated structure which is characteristic of the MAX ternary compound. The micrograph with a lower magnification is displayed in Fig. 6(c) which shows a dense surface with a laminated structure for the product obtained from Reaction (1) with $x=0.7$.

SEM micrographs of Fig. 7(a) and (b) present the typical fracture morphology of the as-synthesized $(Cr,V)_2AlC/Al_2O_3$ composites. The plate-like $(Cr,V)_2AlC$ grains with a thickness of about 0.2 μm are observed and the laminated feature is evident. Fig. 7(c) shows the dense microstructure of a $(Cr_{0.3}V_{0.7})_2AlC/Al_2O_3$ solid solution composite, which experienced substantial melting during the SHS process.

For the synthesized Al_2O_3-added $(Ti_{1-x}V_x)_2AlC$ with $x\geq0.5$ and $(Cr_{1-y}V_y)_2AlC$ with $y\geq0.4$, considerable melting of the samples during combustion led to the formation of almost fully-dense products. By the Archimedes method, the density of dense $(Ti,V)_2AlC/Al_2O_3$ composites is in the range of 4.12–4.31 g/cm^3. For the dense $(Cr,V)_2AlC/Al_2O_3$ products obtained in this study, the density of 4.53–4.78 g/cm^3 was measured. The Vickers hardness of the $(Ti_{0.5}V_{0.5})_2AlC/Al_2O_3$ composite with an indentation load of 9.8 N is approximately 4.8 GPa and the fracture toughness is about 7.2 MPa m$^{1/2}$. For the $(Cr_{0.5}V_{0.5})_2AlC/Al_2O_3$ composite, the Vickers hardness and fracture toughness are 6.3 GPa and 9.7 MPa m$^{1/2}$, respectively. When compared with these properties of Ti_2AlC and Cr_2AlC [39,40], the strengthening and toughness effect is confirmed.

4. Conclusions

Preparation of two Al_2O_3-added MAX solid solutions, $(Ti_{1-x}V_x)_2AlC$ and $(Cr_{1-y}V_y)_2AlC$, with V contents in terms of x and y from 0.1 to 0.7 was conducted by combustion synthesis involving aluminothermic reduction of TiO_2, V_2O_5 and Cr_2O_3. For both reaction systems, combustion exothermicity of the reactant mixture increased with increasing V_2O_5 for the formation of $(Ti,V)_2AlC$ and $(Cr,V)_2AlC$ with a higher V proportion, which enhanced the phase conversion from the reactants to final products. For the production of $(Ti_{1-x}V_x)_2AlC$, successful ignition and full phase evolution were achieved in the cases of $x\geq0.4$. However, the formation of $(Cr_{1-y}V_y)_2AlC$ with $y=0.1-0.7$ was feasible by the SHS process, due to the higher exothermicity for reduction of Cr_2O_3 in comparison to TiO_2. The XRD patterns and calculated lattice parameters of the products confirmed the formation of solid solutions with different V contents. SEM micrographs illustrated that both types of solid solution composites are composed dominantly of plate-like grains closely stacked into a laminated structure. Moreover, considerable melting of the samples during combustion led to the yield of almost fully-dense products. The solid solution strengthening effect was justified by the measured Vickers hardness and fracture toughness of the end products.

Acknowledgments

This research was sponsored by the National Science Council of Taiwan, ROC, under the Grant of NSC 100-2221-E-035-074-MY2. Authors are grateful for the Precision Instrument Support Center of Feng Chia University in providing the measurement facilities.

References

[1] M.W. Barsoum, The $M_{N+1}AX_N$ phases: a new class of solids; thermodynamically stable nanolaminates, Progress in Solid State Chemistry 28 (2000) 201–281.
[2] M.W. Barsoum, D. Brodkin, T. El-Raghy, Layered machinable ceramics for high temperature applications, Scripta Materialia 36 (5) (1997) 535–541.
[3] Z.J. Lin, M.S. Li, Y.C. Zhou, TEM investigations on layered ternary ceramics, Journal of Materials Science and Technology 23 (2) (2007) 145–165.
[4] P. Eklund, M. Beckers, U. Jansson, H. Högberg, L. Hultman, The $M_{n+1}AX_n$ phases: materials science and thin-film processing, Thin Solid Films 518 (2010) 1851–1878.
[5] M.W. Barsoum, T. El-Raghy, Synthesis and characterization of a remarkable ceramic: Ti_3SiC_2, Journal of the American Ceramic Society 79 (7) (1996) 1953–1956.
[6] N.V. Tzenov, M.W. Barsoum, Synthesis and characterization of Ti_3AlC_2, Journal of the American Ceramic Society 83 (4) (2000) 825–832.
[7] Z.J. Lin, M.J. Zhuo, Y.C. Zhou, M.S. Li, J.Y. Wang, Microstructural characterization of layered ternary Ti_2AlC, Acta Materialia 54 (2006) 1009–1015.
[8] Z.J. Lin, Y.C. Zhou, M.S. Li, Synthesis, microstructure, and properties of Cr_2AlC, Journal of Materials Sciences and Technology 23 (6) (2007) 721–746.
[9] Z.J. Lin, M.J. Zhou, M.S. Li, J.Y. Wang, Y.C. Zhou, Synthesis and microstructure of layered-ternary Ti_2AlN ceramic, Scripta Materialia 56 (2007) 1115–1118.
[10] B. Manoum, F. Zhang, S.K. Saxena, S. Gupta, M.W. Barsoum, On the compression behavior of $(Ti_{0.5}, V_{0.5})_2AlC$ and $(Ti_{0.5}, Nb_{0.5})_2AlC$ to quasi-hydrostatic pressures above 50 GPa, Journal of Physics: Condensed Matter 19 (2007) 246215.
[11] S. Dubois, G.P. Bei, C. Tromas, V. Gauthier-Brunter, P. Gadaud, Synthesis, microstructure, and mechanical properties of $Ti_3Sn_{(1-x)}Al_xC_2$ MAX phase solid solutions, International Journal of Applied Ceramic Technology 7 (2010) 719–729.
[12] Y.L. Du, Z.M. Sun, H. Hashimoto, M.W. Barsoum, Theoretical investigations on the elastic and thermodynamic properties of $Ti_2AlC_{0.5}N_{0.5}$ solid solution, Physics Letters A 374 (2009) 78–82.

[13] J.C. Schuster, H. Nowotny, C. Vaccaro, The ternary systems: Cr–Al–C, V–Al–C, and Ti–Al–C and the behavior of H-phases (M_2AlC), Journal of Solid State Chemistry 32 (1980) 213–219.
[14] Z. Sun, R. Ahuja, J.M. Schneider, Theoretical investigation of the solubility in (M_xM_{2-x}')AlC (M and M′ = Ti, V, Cr), Physical Review B 68 (2003) 224112.
[15] S. Gupta, M.W. Barsoum, Synthesis and oxidation of V_2AlC and ($Ti_{0.5}$, $V_{0.5}$)$_2$AlC in air, Journal of The Electrochemical Society 151 (2) (2004) D24–D29.
[16] I. Salama, T. El-Raghy, M.W. Barsoum, Synthesis and mechanical properties of Nb_2AlC and (Ti,Nb)$_2$AlC, Journal of Alloys and Compounds 347 (2002) 271–278.
[17] F.L. Meng, Y.C. Zhou, J.Y. Wang, Strengthening of Ti_2AlC by substituting Ti with V, Scripta Materialia 53 (2005) 1369–1372.
[18] W.B. Tian, Z.M. Sun, H. Hashimoto, Y.L. Du, Synthesis, microstructure and properties of ($Cr_{1-x}V_x$)$_2$AlC solid solutions, Journal of Alloys and Compounds 484 (2009) 130–133.
[19] W. Yu, S. Li, W.G. Sloof, Microstructure and mechanical properties of a $Cr_2Al(Si)C$ solid solution, Materials Science and Engineering A 527 (2010) 5997–6001.
[20] Y.C. Zhou, J.X. Chen, J.Y. Wang, Strengthening of Ti_3AlC_2 by incorporation of Si to form $Ti_3Al_{1-x}Si_xC_2$ solid solutions, Acta Materialia 54 (2006) 1317–1322.
[21] B. Manoun, S.K. Saxena, G. Hug, A. Ganguly, E.N. Hoffman, M. W. Barsoum, Synthesis and compressibility of $Ti_3(Al,Sn_{0.2})C_2$ and $Ti_3Al(C_{0.5},N_{0.5})_2$, Journal of Applied Physics 101 (2007) 113523.
[22] J. Zhu, N. Han, A. Wang, Synthesis, microstructure and mechanical properties of (Ti_{1-x},Nb_x)$_2$AlC/Al_2O_3 solid solution composites, Materials Science and Engineering A 538 (2012) 7–12.
[23] J. Yang, L. Pan, W. Gu, T. Qiu, Y. Zhang, S. Zhu, Microstructure and mechanical properties of in situ synthesized (TiB_2 + TiC)/Ti_3SiC_2 composites, Ceramics International 38 (2012) 649–655.
[24] J.F. Zhu, L. Ye, L.H. He, Effect of Al_2O_3 on the microstructure and mechanical properties of Ti_3AlC_2/Al_2O_3 in situ composites synthesized by reactive hot pressing, Ceramics International 38 (2012) 5475–5479.
[25] W. Zhou, B. Mei, J. Zhu, Rapid synthesis of Ti_3AlC_2/TiB_2 composites by the spark plasma sintering (SPS) technique, Ceramics International 35 (2009) 3507–3510.
[26] A.G. Merzhanov, Combustion processes that synthesize materials, Journal of Materials Processing Technology 56 (1996) 222–241.
[27] G. Liu, J. Li, K. Chen, Combustion synthesis of refractory and hard materials: a review, International Journal of Refractory Metals and Hard Materials (2012) http://dx.doi.org/10.1012/j.ijrmhm.2012.09.002.
[28] G. Liu, K. Chen, H. Zhou, J. Guo, K. Ren, J.M.F. Ferreira, Layered growth of Ti_2AlC and Ti_3AlC_2 in combustion synthesis, Materials Letters 61 (2007) 779–784.
[29] C.L. Yeh, C.W. Kuo, F.S. Wu, Formation of Ti_2AlN by solid-gas combustion synthesis with AlN- and TiN-diluted samples in nitrogen, International Journal of Applied Ceramic Technology 7 (6) (2010) 730–737.
[30] C.L. Yeh, C.W. Kuo, Effects of Al and Al_4C_3 contents on combustion synthesis of Cr_2AlC from Cr_2O_3-Al-Al_4C_3 powder compacts, Journal of Alloys and Compounds 509 (2011) 651–655.
[31] C.L. Yeh, J.H. Chen, Combustion synthesis of $Ti_3Si_{1-x}Al_xC_2$ solid solutions from TiC-, SiC-, and Al_4C_3-containing powder compacts, Journal of Alloys and Compounds 509 (2011) 7277–7282.
[32] C.L. Yeh, C.W. Kuo, F.S. Wu, Effects of TiC and TiN addition on combustion synthesis of $Ti_2AlC_{0.5}N_{0.5}$ solid solutions, Journal of Alloys and Compounds 504 (2010) 386–390.
[33] M. Binnewies, E. Milke, Thermochemical Data of Elements and Compounds, Wiley-VCH Verlag GmbH, Weinheim, New York, 2002.
[34] C.L. Yeh, J.Z. Lin, Combustion synthesis of Cr–Al and Cr–Si intermetallics with Al_2O_3 additions from Cr_2O_3–Al and Cr_2O_3–Al–Si reaction systems, Intermetallics 33 (2013) 126–133.
[35] A.G. Evans, E.A. Charles, Fracture toughness determinations by indentation, Journal of the American Ceramic Society 59 (1976) 371–372.
[36] C.T. Rios, A.A. Coelho, W.W. Batista, M.C. Gonçalves, R. Caram, ISE and fracture toughness evaluation by Vickers hardness testing of an Al_3Nb–Nb_2Al–AlNbNi in situ composite, Journal of Alloys and Compounds 472 (2009) 65–70.
[37] T.P. Ivleva, A.G. Merzhanov, Three-dimensional spinning waves in the case of gas-free combustion, Doklady Physics 45 (2000) 136–141.
[38] C.A. Wang, A. Zhou, L. Qi, Y. Huang, Quantitative phase analysis in the Ti–Al–C ternary system by X-ray diffraction, Powder Diffraction 20 (2005) 218–223.
[39] X.H. Wang, Y.C. Zhou, Layered machinable and electrically conductive Ti_2AlC and Ti_3AlC_2 ceramics: a review, Journal of Materials Science and Technology 26 (5) (2010) 385–416.
[40] Z. Lin, Y. Zhou, M. Li, Synthesis, microstructure, and property of Cr_2AlC, Journal of Materials Science and Technology 23 (6) (2007) 721–746.